Host-guest binding selectivity of ethylated pillar[5]arene (EtP5A) towards octane, 1,7-octadiene, and 1,7-octadiyne: a computational investigation

Adel Krid, Lotfi Belkhiri, Hamza Allal, Aleksey Kuznetsov, Abdou Boucekkine

Host-Guest Binding Selectivity of Ethylated Pillar[5]arene (EtP5A) towards Octane, 1,7-Octadiene, and 1,7-Octadiyne: A Computational Investigation

Adel Krid,[a,b] Lotfi Belkhiri,[a,b*] Hamza Allal,[c] Aleksey Kuznetsov,[d] Abdou Boucekkine[e]

[a] Laboratoire de Physique Mathématique et Subatomique LPMS, Département de Chimie, Université des Frères Mentouri, 25017 Constantine, Algeria.

[b] Centre de Recherche en Sciences Pharmaceutiques CRSP, Zone d'activité ZAM, Nouvelle Ville, Constantine, Algeria.

[c] Département génie mécanique, Faculté de Technologie, Université 20 Aout 1955 Skikda, Algeria

[d] Department of Chemistry, Universidad Técnica Federico Santa Maria, Av. Santa Maria 6400, Vitacura, 7660251, Santiago, Chile.

[e] Univ Rennes, ISCR UMR 6226 CNRS, Campus de Beaulieu, F-35042 Rennes Cedex, France.

Corresponding author

*Email (L. Belkhiri): lotfi.belkhiri@umc.edu.dz

Abstract

Host–guest binding selectivity of the perethylated pillar[5]arene (EtP5A) macrocycles with aliphatic modified hydrocarbons, *i.e.*, octane, 1,7-octadiene, and 1,7-octadiyne as guests, has been investigated computationally employing molecular docking simulations. Density Functional Theory (DFT) investigations were also performed on these host-guest complexes using the dispersion-corrected approach BLYP-D3(BJ)/TZP/COSMO calculations as implemented in the ADF program and two dispersion-corrected density functionals, ωB97XD and B97D, along with the 6-311G* basis set, coupled with the PCM solvation model as implemented in the Gaussian software. We performed analysis of the frontier molecular orbitals (FMO) and Natural Bond Orbitals (NBO), Energy Decomposition Analysis (EDA), and Non-Covalent Interaction (NCI-RDG) analysis. The study sheds light on the structures and binding energetics of EtP5A with the above-mentioned guests as well as on the physicochemical nature of the noncovalent interactions involved in these host-guest inclusion complexes. Based on the docking simulations, the EtP5A host revealed slightly better binding ability in the complex with the alkyne guest than with the octane and alkene, as corroborated by the EDA analysis. The results showed that the complexation of EtP5A with the hydrocarbons is mainly governed by the interplay of electrostatic interactions and dispersive noncovalent interactions. These results agree well with NCI-RDG and NBO analysis showing that host−guest binding interactions result predominantly from electrostatic CH···π and van der Waals interactions, the H-bonding being weak or not observed. The results obtained using different computational methods were found to be in good agreement and complementary.

Keywords: Host-Guest, Pillar[5]arene, Inclusion Complexes, Molecular Docking, DFT, NCI-RDG, NBO.

1. Introduction

During the last two decades, molecular recognition via intermolecular weak interactions, involving host-guest inclusion complex formation with supramolecular macrocyclic compounds, such as cucurbit[n]urils, calix[n]arenes, cyclodextrins, cyclophanes, cyclopeptides, and pillar[n]arenes, has become an interesting new route to construct sophisticated and precisely modelled biological systems with multiple functions [1-6]. In particular, pillar[n]arenes which were first reported in 2008 [7] have attracted considerable attention due to their significant importance in biomedical applications, biology, chemistry, physics, material science, nanotechnology, and environmental applications [8–15]. There exists ever-growing interest toward the usage of macrocyclic molecules as hosts to encapsulate drugs, which inherently provides more resistance to the drug degradation [16,17].

As a part of host-guest systems, pillar[n]arenes exhibit multiple binding sites along with ring-like structures [18-20]. Therefore, they can capture and hold guest molecules in their vacant cavities via various noncovalent interactions (NCI) leading to unique supramolecular architectures [21-25]. Indeed, these NCIs arise from hydrogen bonds, charge transfer, van der Waals interactions, and electrostatic interactions between molecules that can exhibit molecular complementarity and thus the NCIs facilitate the accommodation of a wide variety of neutral and charged guest molecules [26-28]. Notably, the pillar[5]arene (P5A) has been widely investigated experimentally and theoretically, for its facile and efficient synthesis [27-34] and its remarkable host-guest properties with different guest molecules as well as for its supramolecular assembly characteristics [35–39]. The pillar[5]arene macromolecules are made up of hydroquinone units linked by methylene bridges functionalized with multifarious substituents, *e.g.*, hydroxyl, alkoxy, or ethyl groups, as shown in Figure 1.

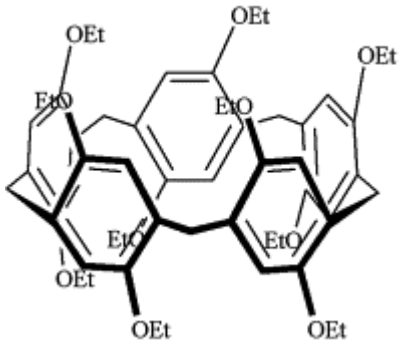

Figure 1. Structure of the ethylated pillar[5]arene (EtP5A).

In 2010, Li et *al*. [40] reported the change of the complexation selectivity of alkylated pillar[5]arenes (P5As) towards the neutral 1,4-bis(imidazol-1-yl)butane guest with the increase of alkyl chain length and showed this inclusion complex to exhibit potent host-guest interactions with the largest association constant,

ca. 10^{-4} M^{-1}. Furthermore, EtP5A host-guest complexes with neutral guests including *n*-alkanes [23-26], haloalkanes [41-43] or unsaturated aliphatic hydrocarbons [44] have been investigated using adsorptive separation experiments. It has been shown that selective host-guest binding is profoundly influenced by noncovalent interactions [23,45]. Interestingly, Venkataramanan et *al.* [26] reported a computational study on the nature of host–guest interactions between the hexane and pillar[5]arene and its quinone modified pillararenes using the dispersion-corrected DFT and wave function methods. The authors showed that the introduction of quinone in pillararene prompted flexibility in structure and the increase of the electrophilicity and the binding ability of pillararenes towards linear guest molecules.

In particular, the selectivity of EtP5A towards neutral aliphatic and linear hydrocarbon guests such as octane, 1,7-octadiene, and 1,7-octadiyne, has been investigated experimentally by Hu et *al*. [44]. The authors concluded that the host–guest binding strength increased in accordance with the electronegativity of the guest terminal carbon atom: alkyne > alkene > alkane. At the theoretical level, much effort has been made to achieve deeper understanding of the selective binding of hydrocarbons by the pillar[5]arene host and rationalizing the underlying interactions within its inclusion complexes [10,15,22,27,28,30,33,34].

Motivated by these studies, we report for the first time a detailed theoretical investigation of the selectivity of perethylated pillar[5]arenes towards octane, 1,7-octadiene, and 1,7-octadiyne using the molecular docking approach combined with DFT calculations. We aim to explain the host-guest binding properties and the driving forces responsible for the EtP5A selective complexation towards such aliphatic guests. The study is focused on the nature of interactions within the inclusion complexes formed by the EtP5A and the three neutral hydrocarbon molecules. To thoroughly address this question, we have performed the Energy Decomposition Analysis (EDA) study, and molecular electrostatic potential (MEP) and atoms-in-molecules (AIM) studies were carried out. The results are further ascertained with the noncovalent interactions index-reduced density gradient (NCI-RDG) study. Frontier molecular orbitals (FMOs) and Natural Bonding Orbital (NBO) analyses were performed as well providing other relevant descriptors. The conclusions drawn from the study might shed light on improving the host-guest binding and delivery properties of pillar[n]arenes.

2. Computational details

The three-dimensional EtP5A host-guest complexes including the hydrocarbon molecules, octane, 1,7-octadiene, and 1,7-octadiyne, were generated from the pdb format using Autodock-Vina software [46], which allows to predict the binding free energy of complexes. The EtP5A host was used as a rigid receptor, and Autodock Tools [47] was used to determine the possible rotations of bonds by molecular docking. During the simulation, the ligands (guest molecules) were docked to the EtP5A with box dimensions set to

the grid (22 × 24 × 24) $Å^3$ in volume, and the cartesian coordinates center was set to 0.017, -0.021, and -0.097 Å. The docking configuration with the highest free-energy score (ΔG) was used as the starting geometry conformations for the DFT calculations.

The structures of all species, including the host, the guests, and their three complexes, generated by Autodock Tools docking simulations, were reoptimized in both gas and implicit solvent phases using the DFT approaches as implemented in two quantum chemistry programs: Amsterdam Density Functional ADF2021.107 program release [48,49] and the Gaussian 09 program package [50].

As implemented in the ADF program, the generalized gradient approximation (GGA) BLYP exchange-correlation density functional [51,52] was used along with the Grimme's D3-BJ empirical dispersion correction [53,54]. The D3-BJ correction was used to improve the description of noncovalent interactions, *i.e.*, hydrogen bonding and van der Waals forces. Indeed, several previous post-Hartree-Fock (CCSD(T) and MP2) studies showed that dispersion corrections allow a better assessment of energies for noncovalent interactions [41,51]. For the ADF computations, the all-electron TZP basis set composed of triple-ζ Slater-type orbitals (STO) and augmented by polarization functions was used for all atoms. The solvent (chloroform) effects were introduced via the COSMO (Continuum Screening Model) method [55]. This solvent was chosen due to the fact that it is often used for synthesis and characterization of such EtP5A complexes and various organic compounds [14]. To ensure that the optimized structures are the real minima, vibration analysis based on the harmonic frequency approximation of the optimized structures was performed using ADF single-point calculations at the same BLYP-D3(BJ)/TZP level of theory. To elucidate the nature of the host-guest binding properties in such complexes, the analysis of the noncovalent interactions (NCI) combined with the index-reduced density gradient (RDG), commonly named the NCI-RDG technique, was carried using the MultiWfn program with larger size grids [56], and noncovalent interactions were depicted with the visual molecular dynamics (VMD) software [57].

The energy decomposition analysis (EDA) method developed by Ziegler et *al*. [58], based on the transition-state method developed by Morokuma [59], providing insights into the balance of the different bonding electronic or electrostatic factors at work between the isolated fragments, was used to analyze in a quantitative manner the nature of host-guest noncovalent interactions. The complexation or binding energy (ΔE) between the guest and the host was calculated as follows:

$$\Delta E = E_{Complex} - (E_{Host} + E_{guest}) \qquad (1)$$

where $E_{complex}$, E_{Host}, and E_{guest} are energies of the optimized complex, the host (EtP5A), and the free guest, respectively.

The inclusion phenomenon is accompanied by a geometry distortion which can be described by the strain (deformation) energy ΔE_{strain}. The latter is the energy needed to deform the EtP5A or guest molecules

during the inclusion process. The strain energy was calculated as the energy difference between the molecule (host or the guest) within the inclusion complex ($E^{complex}$), and its free optimized components (E^{free}) given by the equation 2:

$$\Delta E_{strain} = E^{complex} - E^{free} \quad (2)$$

The energy decomposition analysis (EDA) was performed considering the binding energy of all host-guest complexes as a combination of several meaningful terms: the Pauli electrostatic or repulsion energy (ΔE_{Pauli}), the electrostatic energy (ΔE_{Elstat}), the orbital interaction energy (ΔE_{Orbt}), and the dispersion energy (ΔE_{Disp}), as given by the equation 3:

$$\Delta E_{bind} = \Delta E_{Pauli} + \Delta E_{Elstat} + \Delta E_{Orbt} + \Delta E_{Disp} \quad (3)$$

The method of noncovalent interaction-reduced density gradient (NCI-RDG) analysis provides the graphical visualization of the regions where noncovalent interactions occur in real-space and was demonstrated to be capable of distinguishing hydrogen bonds, van der Waals interactions, and repulsive steric interactions through simple color patches [22,60,61].

Using the Gaussian 09 program, two DFT functionals including dispersion corrections, ωB97XD [62] and B97D [63], were used in combination with the full-electron 6-311G* split-valence basis set with one set of polarization functions on heavier atoms [64,65]. These computational approaches are further referred to as ωB97XD/6-311G* and B97D/6-311G*. Geometry optimizations and frequency calculations were performed with the implicit effects of chloroform taken into account (dielectric constants $\varepsilon(CHCl_3)$ = 4.7113) using the self-consistent reaction field IEF-PCM method [66], with the UFF default model used in the Gaussian 09 package, with the electrostatic scaling factor α set to 1.0.

To ensure that the Basis Set Superposition Error (BSSE) does not change significantly these energies, the binding energies including BSSE at the ωB97XD/6-311G* level were calculated for the complexes 1-3 in the gas phase *(vide infra).*

In order to gain further insights into the nature of bonding within the complexes and to examine the electronic features, the natural bond orbital (NBO) [67] analysis as implemented in Gaussian 09 program was carried out at the same level of theory for all optimized structures. Molecular orbitals (MOs) for the ground state structures were calculated with the implicit solvent effects included as well using the ωB97XD/6-311G* and B97D/6-311G* optimized geometries. Also, molecular electrostatic potential (MEP) was calculated with the implicit solvent effects included using the ωB97XD/6-311G* and B97D/6-311G* optimized geometries. Complex structures and MOs were visualized using OpenGL version of Molden 5.8.2 visualization software [68]. Avogadro, version 1.1.1, was used to visualize the molecular electrostatic potential (MEP) maps [69,70].

3. Results and discussions

3.1. Molecular docking simulations

The molecular geometries of the inclusion complexes **1**, **2**, and **3** including the EtP5A host and the hydrocarbon ligands as guest, *i.e.*, octane, 1,7-octadiene and 1,7-octadiyne, respectively, were generated by Autodock Tools docking simulations and are shown on Figure 2. The binding energies (scores) ΔG as computed by docking simulations are also reported on Figure 2.

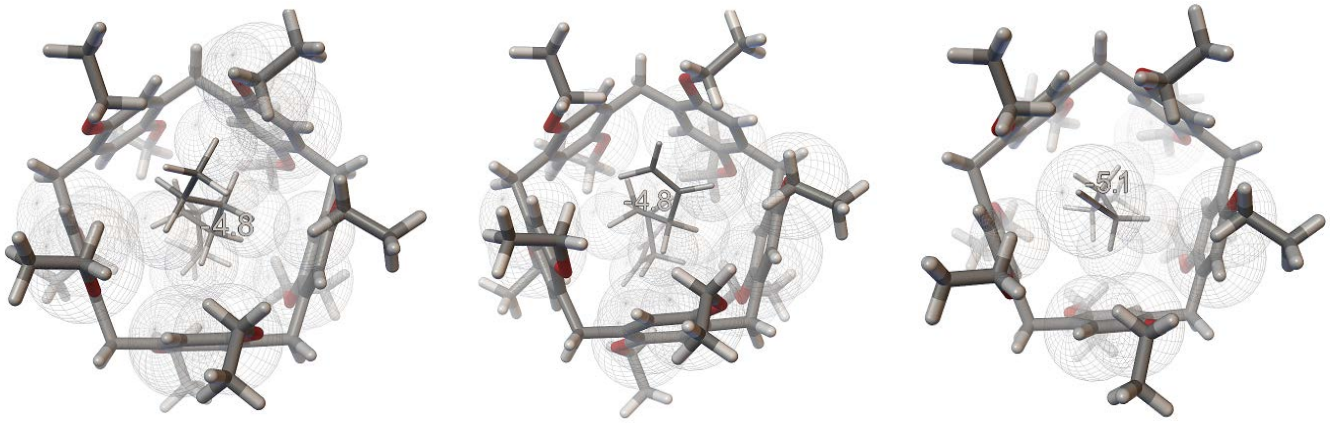

Complex 1 (–4.8) **Complex 2 (**–4.8) **Complex 3 (**–5.1)

Figure 2. Autodock Tools simulation of inclusion complexes showing the non-covalent interactions (with octane (left), 1,7-octadiene (middle), and 1,7-octadiyne (right)). Docking energies ΔG (kcal/mol) are given between parentheses.

As shown in Figure 2, all ligands are completely docked in the cavity of the host molecule in the same manner, forming the inclusion complexes with 1:1 stoichiometric ratio. The docking energy results show the binding energy (ΔG) values to be all negative suggesting that the formation of these inclusion complexes is thermodynamically favored, with the ligand 3 (1,7-octadiyne) having slightly more favored binding energy (–5.1 kcal/mol) relative to the octane and 1,7-octadiene (–4.8 kcal/mol). Analysis of interactions between EtP5A and guest molecules (Figure 2) shows no evidence for hydrogen bond formation and only van der Waals and CH···π interactions should mainly contribute to the major host-guest interactions in these inclusion complexes.

3.2. DFT analysis

3.2.a. Host-guest binding energies

All geometry structures of host-guest species generated by Autodock Tools docking simulations were reoptimized using the BLYP-D3(BJ)/TZP approach. The top and side views of the DFT optimized

geometries for the host molecule (EtP5A) in solvated phase (COSMO) are shown in Figure 3.

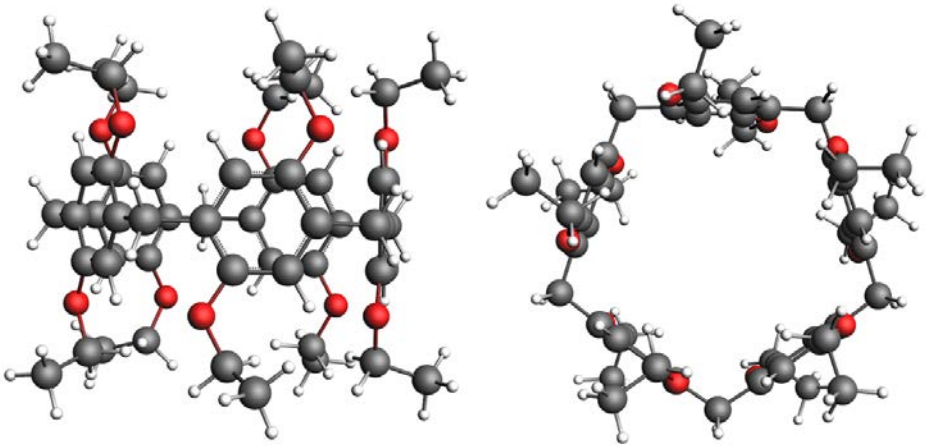

Figure 3. Top and side view of the BLYP/D3(BJ)/COSMO optimized EtP5A host molecular structure.

The lowest-energy DFT optimized structures of the host-guest complexes in solvated phase (COSMO) are shown in Figure 4, and their structures optimized with the implicit solvent effects using the ωB97XD/6-311G* and B97D/6-311G* approaches, both side and top views, are given in Figures S1 and S2 (See Supplementary Information). The optimized structures using the different DFT approaches are similar.

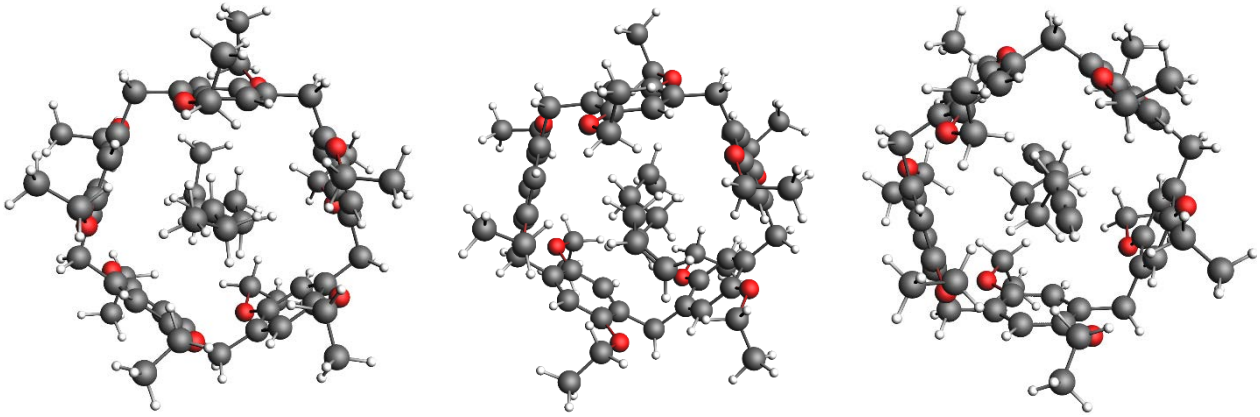

1 **2** **2**

Figure 4. BLYP/D3(BJ)/COSMO optimized geometry of the host-guest complexes 1, 2, 3.

The BLYP-D3(BJ)/TZP binding energies reported in Table 1 were computed in both gas and implicit solvent phases. The BLYP-D3(BJ)/TZP results (Table 1) are compared to the ωB97XD/6-311G* and B97D/6-311G* results.

Table 1: Binding energies ΔE (kcal/mol) of the host-guest complexes in the gas and implicit solvent phases.

Complex	ΔE_{gas}	ΔE_{solv}	ΔE_{solv}	
	BLYP-D3(BJ)/TZP		ωB97XD/6-311G*	B97D/6-311G*
Complex 1	−31.75	−29.37	−39.11	−32.96
Complex 2	−34.15	−30.70	−39.49	−33.13
Complex 3	−37.13	−35.52	−40.68	−34.25

As compared to the docking simulation results (Figure 2), Table 1 shows all DFT binding energies to be negative, corresponding to the bound host-guest complexes, thus indicating that the inclusion phenomenon is stabilized and thermodynamically favored. The computed BLYP-D3(BJ) gas-phase binding energies are higher than those obtained in the solvent phase, by 1.61-3.45 kcal/mol. Notably, the three DFT methods show that the complex 3, associating the EtP5A and 1,7-octadiyne molecule, is found to be the most stable one in comparison to the two others.

Furthermore, our DFT computed binding energies agree well with the experimental trend observed in previous works suggesting that host–guest binding strength increased as follows: alkyne > alkene > alkane. Indeed, as reported by Hu et *al*. [44], the EtP5A/1,7-octadiyne complex gives the largest association constant ($K_a = 82 \pm 5$ mol^{-1} L), compared to the congener EtP5A/1,7-octadiene with the constant 6.8 times lower. In the cases of the unsaturated hydrocarbon (octane), the constant was not accurately measured and was found to be too low ($K_a < 2$ mol^{-1} L) [44].

Indeed, the computed binding energies of the complexes using the ωB97XD/6-311G* and B97D/6-311G* approaches steadily increase from the complex 1 to complex 3, the latter being the most stable, in good agreement with the BLYP-D3(BJ)/TZP results. One can notice that the ωB97XD/6-311G* binding energies are by *ca*. 6.25 kcal/mol larger than the B97D/6-311G* values (Table 2). Despite these differences between the three used DFT approaches, the relative stability of the host-guest complexes is predicted to behave in the same way. Interestingly, the size of guest molecules seems to play an important role in the inclusion process. Indeed, the 1,7-octadiyne has less steric effects due to the sp-hybridization of its terminal carbon, which could favor the inclusion process.

The strain energy as given by the equation 2 (see computational details) was computed using the BLYP-D3(BJ)/TZP approach in solvated phase and reported as relative deformation energies ΔE_{strain} in Table 2 for both the guest and host molecules, both in free and in distorted (complexes 1-3) configurations.

Table 2: BLYP-D3(BJ)/COSMO total bonding energy TBE (eV) and strain energies (ΔE_{strain}) of the host and guest.

Energy (eV)	Complex	Free	ΔE_{strain} (kcal/mol)
Host			
1	-783.982	-784.049	0.067 (1.55)
2	-783.989	-784.049	0.059 (1.37)
3	-784.022	-784.049	0.026 (0.61)
Guest			
Octane	-133.791	-133.834	0.043 (1.00)
Octadiene	-100.740	-100.775	0,035 (0.82)
Octadiyne	-117.779	-117.809	0,030 (0.70)

From the results of Table 2, it appears that the host (EtP5A), referring to the complex 3 (EtP5A/1,7-octadiyne), exhibits slightly lower strain energy ΔE_{strain} (0.61 kcal/mol) relative to the complex 1 and 2 associating the octane and 1,7-octadiene, respectively. Previous studies on similar stable inclusion complexes showed low strain energy for both the guest and host molecule [22,42,71].

Moreover, regarding the strain energies ΔE_{strain} of the three guest molecules, the alkyne molecule shows the lowest deformation energy (0.70 kcal/mol) relative to the alkane and alkene, thus resulting in a better guest molecule inclusion in the cavity of the host. These results are in line with the higher association constant (K_a) between the alkyne (guest) and EtP5A (host) within the complex 3, which was observed to be 6.8 times larger than the association constant measured for alkene in the complex 2, while for the alkane-EtP5A complex 1, the association constant is much weaker [44].

3.2.b. Frontier molecular orbital analysis

It was established that for a macromolecule to act as a controlled delivery system, it should reversibly adsorb and release a ligand (*e.g.*, a drug) via a kinetically controllable process [9,22,66]. To understand the kinetic stability of these inclusion complexes, the E_{gap}, the energy difference between the HOMO (highest occupied molecular orbital) and LUMO (lowest unoccupied molecular orbital) was computed using the ADF/BLYP-D3BJ method. The computed HOMO and LUMO energies (eV), E_{gap} (eV), and the global dipole moment μ (Debye) for all the species in the solvent phase are provided in Table 3.

Table 3: BLYP-D3(BJ)/TZP calculated HOMO, LUMO, and HOMO-LUMO gap energies (eV) as well as global dipole moment μ (Debye) for the free and distorted* host, guests, and their complexes in the implicit solvent phase.

	EtP5A	octane	1,7-	1,7-	Complex	Complex	Complex

			octadiene	octadiyne	1	2	3
HOMO	–4.119	–7.071	–6.056	–6.421	–4.302	–4.342	–4.378
LUMO	–0.957	+0.126	–0.706	–0.284	–1.116	–1.160	–1.245
E_{gap} (eV)	3.162	7.197	5.350	6.137	3.186	3.182	3.133
μ (D)	0.059	0.055	0.887	1.636	3.236	3.092	1.600
μ (D) Host*					2.999	3.341	1.637
μ (D) Guest*					0.094	0.521	0.142

As shown in Table 3, the HOMO-LUMO gap for the inclusion complexes is significantly smaller than for the hydrocarbons (guests), which indicates that complexes formation can be kinetically controllable, in good agreement with previous studies [9,22,66]. Moreover, complexes 1, 2, and 3 show similar energy gaps, *ca*. 3.15 eV, close to the host EtP5A (3.16 eV). The same trend is obtained using the ωB97XD and B97D functionals (see Tables S1 and S2), showing that all complexes have the HOMO–LUMO gaps noticeably smaller than the guest hydrocarbons, again in good agreement with the BLYP/D3(BJ) results. HOMO and LUMO of the complexes are mainly those of the host molecule as it can be seen in Figure 5.

Moreover, it appears that the computed global dipole moment (μ) of the free guest decreases with the change of the terminal carbon atom hybridization, $sp > sp^2 > sp^3$. Indeed, the higher electronegativity of the sp-hybridized terminal carbons on 1,7-octadiyne was reported, that resulting in stronger binding between alkyne and EtP5A compared to the other guests [44]. For the saturated hydrocarbon (octane), very weak binding is observed as can be seen from the lower value of the association constant [44]. Interestingly, the dipole moment trend is inverted for the inclusion complexes leading to the highest dipole moment (3.236 D) for the octane-containing (sp^3) complex 1. It can be seen from Table 4 that the dipole moment of the host in its distorted geometry (within complexes 1-3) exhibit the same trend as the dipole moment of the complexes, increasing from 0.059 to 1.637 D when passing from the free to the inclusion structure (complex 3).

This increase of dipole moment from the host and guest to the complexes is also closely related to the enhancement of induced dipole-dipole interactions (van der Waals interactions) between the guest and host molecules which are, in cooperative multiple noncovalent interactions, essential for realizing such strong complexations. Therefore, it is likely that the latter interactions play a significant role in stabilizing the inclusion process. This point will be detailed later in the text.

The FMO plots for the complexes obtained at the BLYP/D3(BJ) level are shown in Figure 5. For all the complexes, the HOMO density is predominantly located on the host moiety, with no contributions from

the guest molecules. This indicates that no electronic charge transfer occurs within such host-guest inclusion complexes, and the encapsulated ligand does not alter the electronic structure of the host significantly. This result suggests that the encapsulation occurs by a pure physical adsorption process [10].

The comparison with the ωB97XD/6-311G* and B97D/6-311G* computed plots of the frontier MOs (cf. Figs. S3 and S4) shows good agreement with the BLYP-D3(BJ)/TZP obtained plots (Figure 5). Even with larger isosurface value, 0.01 au, it is clearly seen that both HOMO and LUMO of the complexes are dominated by the host moiety contributions, with very small, if any, guest contributions.

The binding energy values (Tables 2 and S1), along with the HOMO and LUMO plots, indicate that the inclusion process is dominated by rather physical adsorption and suggest that the EtP5A can be used as a reversible host for the considered hydrocarbon molecules as reported for delivery systems [72].

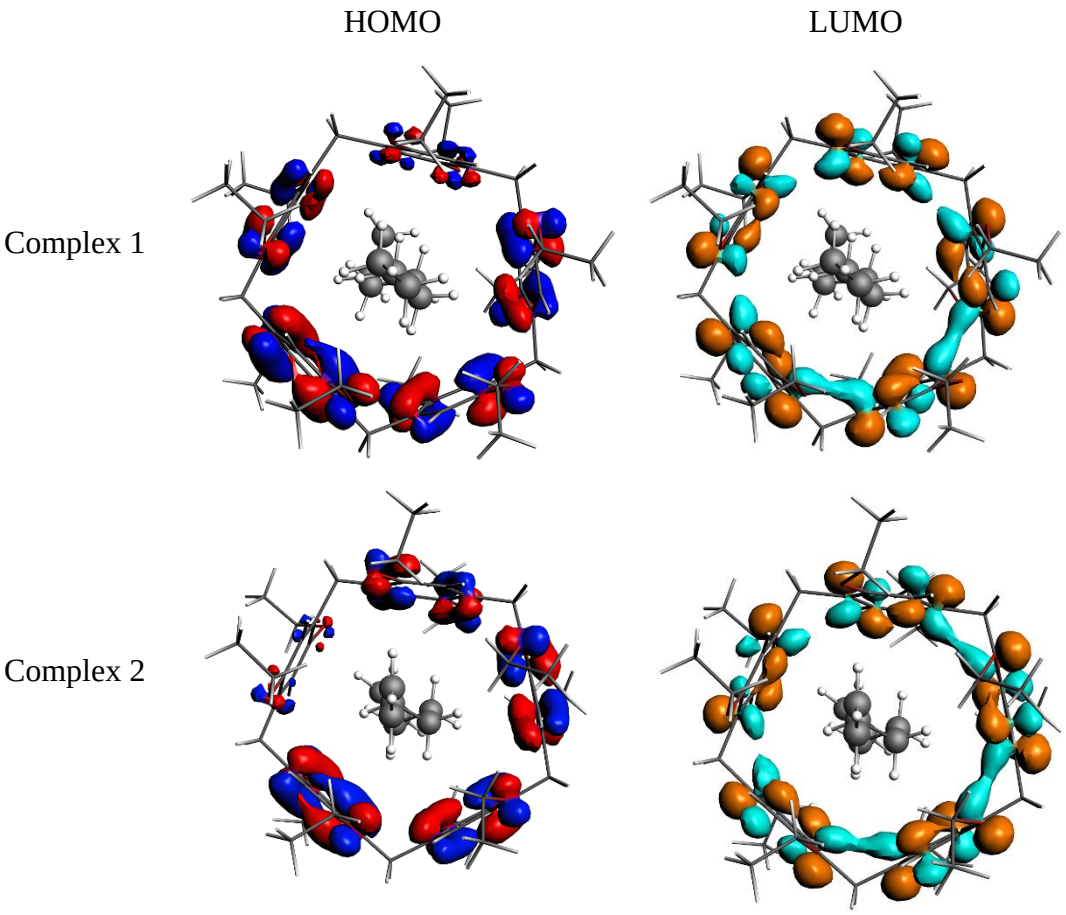

Complex 3

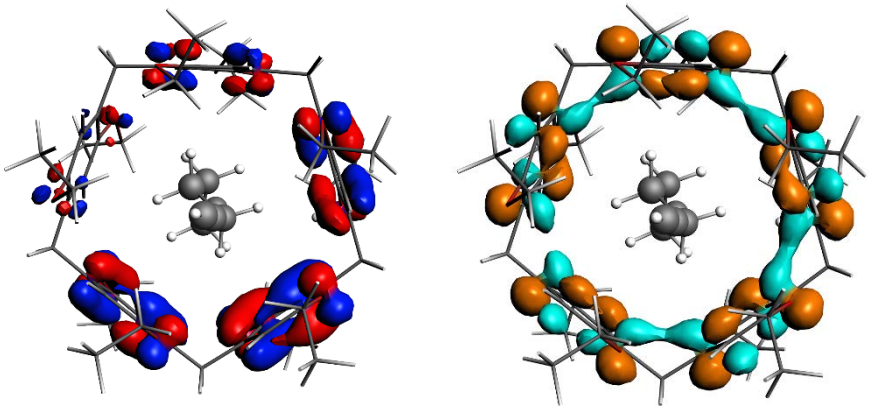

Figure 5. BLYP-D3 (BJ)/COSMO HOMO and LUMO of the host-guest inclusion complexes (isosurface value is ± 0.03 au).

3.2.c. Molecular Electrostatic Potential (MEP) analysis

Molecular electrostatic potential analysis is a useful tool for studying the charge distribution within the host cavity and orientation of noncovalent bonds in the inclusion complexes [73]. A rationalization of noncovalent intermolecular interactions based on MEP analysis has been carried out using the BLYP-D3(BJ)/COSMO results including the implicit chloroform solvation effects.

Figure 6 displays molecular electron density isosurfaces (0.001 au) of the EtP5A host overlaid, *e.g.*, with MEP of the inclusion complex 2. Similarly, the MEP analysis has been carried out using ωB97XD/6-311G* calculations (Fig. S5).

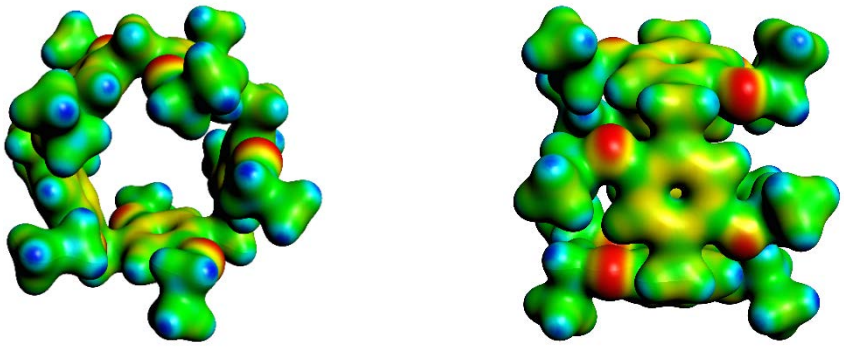

(a) MEP ETP5A

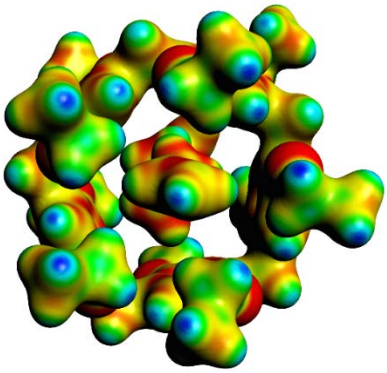

(b) MEP inclusion of complex 2

Figure 6. BLYP-D3(BJ)/COSMO MESP mapped on (a) EtP5A host top and side view, (b) complex 2 (isosurface 0.001 au).

Figure 6 shows that the electrostatic potential surface of the complexes is typically non-uniform. It reveals combination of electron-rich negative regions (depicted in red) corresponding mainly to the oxygen-containing groups, and electron-deficient positive parts (blue) corresponding to ends of the alkyl groups. Such positive regions can be considered as electrophilic sites, and negative regions surrounding the guest molecules in attractive interactions are considered as nucleophilic sites. Indeed, as reported by previous studies [22,42,73,74], these electrostatic properties shown on the EtP5A macromolecule favor stronger attractive host−guest interactions arising from their binding during the inclusion process (Fig. S5). The polarization of the host upon complexation is significant as it can be seen comparing Figures 6a and 6b.

3.2.d. Energy decomposition analysis (EDA)

To shed more light on the contributions of the different components of the interaction energy ΔE_{bind} within the considered host-guest complexes, the energy decomposition analysis (EDA) was performed considering the implicit solvent phase (chloroform) using the BLYP-D3(BJ)/TZP COSMO approach. The total binding energies as well as the decomposition terms (kcal/mol) along with their contributions in percentage (%) are reported in Table 5. The different decomposition terms are given by equation 3 (see Computational details):

$$\Delta E_{bind} = \Delta E_{Pauli} + \Delta E_{elst} + \Delta E_{orb} + \Delta E_{disp} \qquad (3)$$

In Table 4, the percentages (%) are the weights of the different stabilizing terms, electrostatic interactions (ΔE_{elst}), orbital interaction (ΔE_{orb}), and dispersion (the London or van der Waals interactions) (ΔE_{disp}), excluding the Pauli repulsion (ΔE_{Pauli}) destabilizing term from the components of the total binding energy (ΔE_{bind}).

Table 4: BLYP-D3(BJ)/TZP COSMO EDA (kcal/mol) and percentage (%) of the stabilizing contributions in the implicit solvent phase (chloroform) are given between parentheses for the complexes 1-3.

EDA kcal/mol (%)	ΔE_{bind}	ΔE_{Pauli}	ΔE_{elst}	ΔE_{orb}	ΔE_{disp}
Complex 1	–32.97	52.96	–21.43 (24.93)	–12.17 (14.16)	–52.34 (60.01)
Complex 2	–34.95	49.22	–22.00 (26.13)	–12.20 (14,49)	–49.97 (59.36)
Complex 3	–38.20	49.53	–25.45 (29.01)	–13.33 (15.19)	–48.94 (55.79)

As shown in Table 4, the destabilizing Pauli term (ΔE_{Pauli}) is computed to be significantly higher for the complex 1 (52.96 kcal/mol) than for the complexes 2 and 3. This is likely due to the increased steric hindrance caused by the terminal carbon hybridization (sp^3) of the guest molecule (octane). The stabilizing electrostatic (ΔE_{elst}) term is computed to be lower for complexes 1 and 2 than for complex 3, in relation with the higher electronegativity of the terminal carbon of the alkyne (sp). Interestingly, one can notice that the dispersion term (ΔE_{disp}), the dominating effect in the inclusion process, is predicted to be slightly higher in the complex 1 and 2 than in 3. It is noteworthy that regarding the contribution percentage it appears that the dispersion (ΔE_{disp}) term is the most important factor in the stabilizing inclusion process, depending on electronegativity of the terminal atom in this case [41]. Therefore, it appears that the use of dispersion correction is essential in estimating the correct binding energy and to determine the long bonding interactions as stated in the literature [22,41,53,62].

The electrostatic contribution (ΔE_{elst}) for the complexes 1-3 is also predicted to be significantly high, contributing to their stability. Furthermore, this electrostatic term seems to increase with the terminal carbon hybridization change ($sp > sp^2 > sp^3$), being slightly higher for the complex 3 in comparison to the complexes 1 and 2 (29.0 *vs.* 24.9 and 26.1, respectively). The orbital interaction (ΔE_{orb}) term has low contribution in comparison to the other terms and suggests weak charge transfer and polarization interactions within these host-guest complexes.

It appears that electrostatic and dispersion effects play a crucial role in stabilizing such inclusion complexes corroborating well the experimental and theoretical results [22,41,44]. The computed binding energy shows the inclusion complexes to be stable, and thus their formation can occur at room temperature. In order to check this point, Basis Set Superposition Error (BSSE) calculations have been carried out using the Gaussian software at the ωB97XD/6-311G* level in the gas phase. The computed complexation energies with or without the BSSE corrections are reported in Table 5. From this latter table, it follows that taking

into account the BSSE somewhat lowers the binding energy as usual, however, the binding trend remains the same as without BSSE. Notably, the BSSE corrections do not change significantly the energies.

Table 5: ωB97XD/6-311G* BSSE calculation results of the complexes 1-3 in the gas phase.

E, kcal/mol	Complex 1	Complex 2	Complex 3
Complexation energy	–44.34	–44.51	–46.63
+ BSSE correction	–38.35	–38.35	–41.07
BSSE energy	5.99	6.15	5.55

3.2.e. NCI-RDG analysis on the inclusion complexes

The NCI-RDG analysis was carried out to visualize the nature of interactions between the EtP5A (host) and the three hydrocarbon molecules using the program MultiWfn with larger size grids [56]. Figures 7 and 8 display the NCI-RDG mapping of the EtP5A and the corresponding inclusion complexes 1-3, respectively.

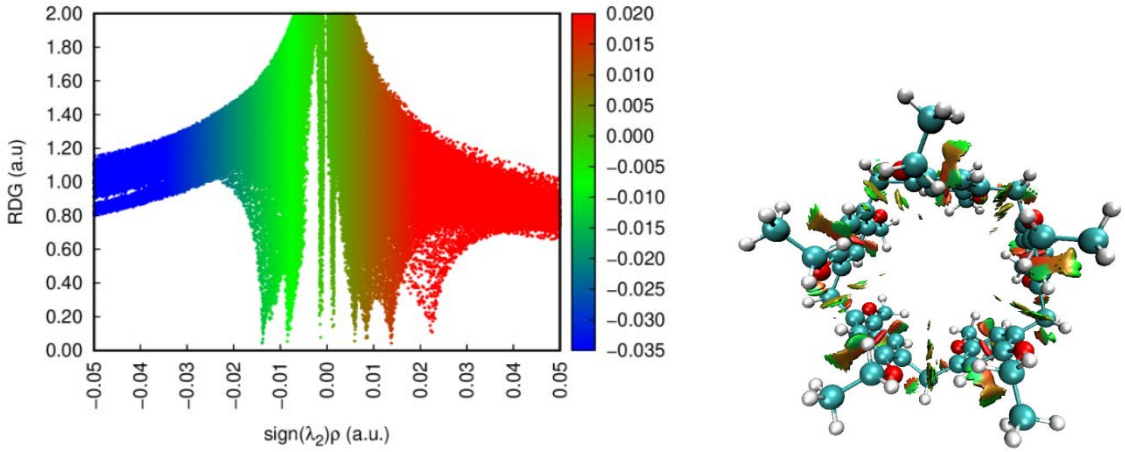

Figure 7. RDG map and NCI isosurfaces for the host (EtP5A) constructed with RGD = 0.5 a.u. (blue–red colors scaling from −0.05 < (λ_2)ρ < 0.05 a.u.).

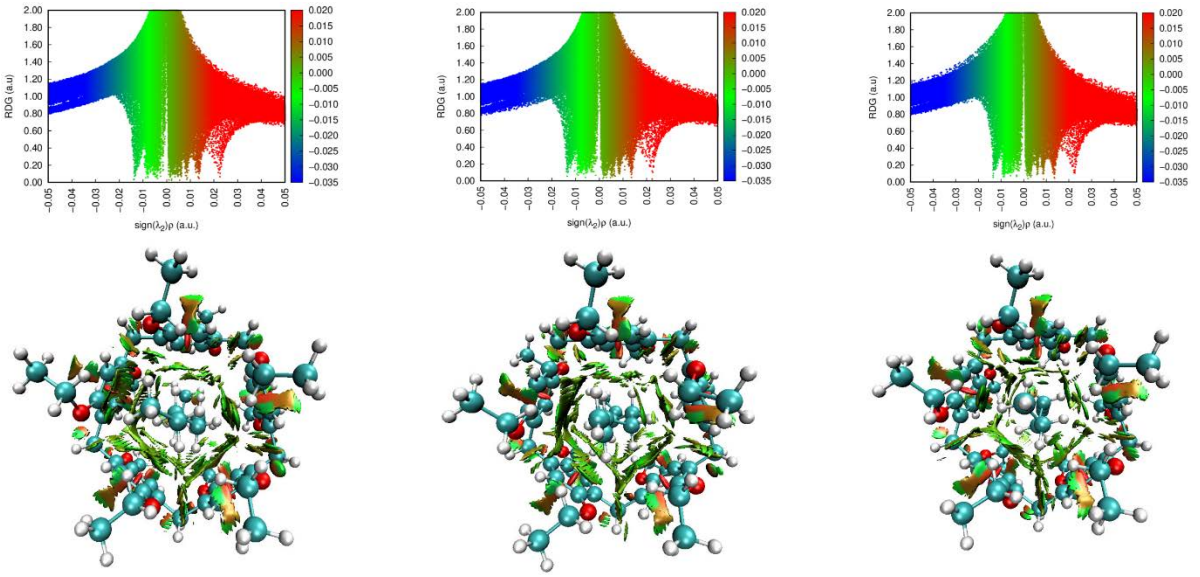

(a) (b) (c)

Figure 8. RDG map and NCI isosurfaces for the inclusion complex 1 (a), complex 2 (b), complex 3 (c) constructed with RGD = 0.5 a.u (colors scaling from $-0.05 < \text{sign}(\lambda_2)\rho < 0.05$ a.u.).

Typically, blue and green color regions are used to represent the stabilizing H-bonding and van der Waals interactions while red color region is used for the destabilizing steric interactions [26,56,59,60]. The interaction types are determined by analyzing the sign of λ_2 which represents the eigenvalues of the Hessian of the electron density at the BCP (bond critical points). As reported by other authors [75,76], for the bonding interactions such as H-bonding, the λ_2 value will always be less than 0 while for the van der Waals type of interactions, $\lambda_2 \leq 0$. The non-bonding interactions like steric repulsions feature $\lambda_2 > 0$.

As shown by the RDG isosurfaces (Figures 7 and 8), the strength and type of noncovalent interactions can be assessed from the product sign $(\lambda_2)\rho$ (ranging from −0.5 to +0.5 au). For the EtP5A macromolecule (Figure 7), the NCI results ($\lambda_2 < 0$) show that the host is stabilized by hydrogen bonds between the oxygen atoms of alkoxy groups and the methylene hydrogens; the red disk area ($\lambda_2 > 0$) is also observed indicating a steric repulsion and at the middle of the benzene rings.

In the inclusion complexes (Figure 8a-c), one can observe green areas between the C–H of terminal carbon atoms in the hydrocarbon guests and the EtP5A host, indicating the existence of van der Waals forces and electrostatic CH···π interactions as pointed out in the literature [26]. The H-bonding is weak as follows from the RDG map (RDG > 0.80). Destabilizing interactions, shown by the red disk area, are also observed indicating steric repulsions and seem to appear at the middle of the benzene rings.

It is noteworthy when passing from Figure 7 to 8, *i.e.*, after the structural reorganization upon encapsulation of guests, that the steric repulsions (red zone) within the host were slightly reduced by van

der Waals stabilizing interactions (green zone). Indeed, one can visualize on NCI isosurfaces the green patches to be evenly distributed inside the EtP5A host molecule in the inclusion complex systems, indicating electrostatic interactions, which are responsible for stabilization of the hydrocarbon molecules inside the EtP5A unit. This phenomenon was also shown by previous studies [21,42,56,59,60], however, it reveals to be quite similar for the three octane (sp^3), 1,7-octadiene (sp^2) and 1,7-octadiyne (sp) inclusion complexes, corroborating the EDA results.

3.2.f. NBO (Natural Bonding Orbital) analysis

With the help of NBO analysis, we can gain significant insights into different types of orbital interactions in the compounds of interest [67]. In general, the NBO analysis is performed by considering the possible interactions between the filled (donor) Lewis-type NBOs and the empty (acceptor) non-Lewis type NBOs. Then, their energetic contributions are computed using second-order perturbation theory. These donor-acceptor interactions lead to a decrease in the localized NBOs occupancy in the idealized Lewis structure and an increase in the occupancy of the empty non-Lewis orbitals. Therefore, such interactions are referred to as 'delocalization' corrections to the zero-order natural Lewis-type structures. The stronger donor-acceptor interactions have higher stabilization energies [67]. The second-order stabilization energy $E^{(2)}$ is calculated using the equation 4:

$$E^{(2)} = q_i \frac{(F_{i,j})^2}{\varepsilon_j - \varepsilon_i}, \qquad (4)$$

In this equation, ε_i and ε_j represent off-diagonal elements and $F_{i,j}$ is the diagonal elements of the NBO Fock matrix, q_i is the donor orbital possession, and $E^{(2)}$ is the energy of stabilization.

Table S3 lists the representative values for the host-guest stabilization energies along with energy differences between donor and acceptor *i* and *j* NBO orbitals and diagonal NBO Fock matrix elements for the complexes 1-3 (with the stabilization energies threshold 0.1 kcal/mol). In Tables S4-S6 the more significant stabilization energy values are listed for the complexes 1-3, respectively (with the stabilization energies threshold more than 0.2 kcal/mol), all of them computed at the ωB97XD/6-311G* level in the implicit $CHCl_3$ solvent.

Analysis of these stabilization energy values for the complexes 1-3 shows the following. (i) For all three complexes, there exist quite numerous stabilizing intramolecular interactions host→guest and guest→host, with the highest interaction energy 0.99 kcal/mol, for the host→guest LP(O)→σ*(C–H) in the complexes 2 and 3. (ii) Host→guest interactions are represented by both π(C-C)→σ*(C–H) and LP(O)→σ*(C–H) type interactions, with the former due to the relatively highly polarizable π–electrons of the benzene rings and the latter due to relatively polarizable (compared to covalent bond electron clouds)

lone-pair electrons of the alkoxy groups. In the complexes 1 and 2, generally the LP(O)→σ*(C–H) type interactions have somewhat higher energies than the π(C-C)→σ*(C–H) type interactions (cf. Tables S4 and S5), whereas in the complex 3 the LP(O)→σ*(C–H) type interactions generally have somewhat lower energies than the π(C-C)→σ*(C–H) interactions (Table S6). (iii) Guest→host interactions are represented by the σ(C-H)→π*(C–C) and σ(C-H)→σ*(C–H) type interactions in the complex 1 (see Table S4), by the π(C-C)→σ*(C–H), σ(C-H)→π*(C–C) and σ(C-H)→ LP(C) type interactions in the complex 2 containing the alkene (Table S5), and by the π(C-C)→σ*(C–H) and σ(C-H)→π*(C–C) type interactions in the complex 3 containing the alkyne (Table S6). The total energy of the guest→host interactions in the complex 3 is higher compared to other two complexes, which can explain higher binding energy in the complex 3.

Conclusions

Computational investigation of the perethylated pillar[5]arene (host) selectivity toward the octane, 1,7-octadiene, and 1,7-octadiyne (guests) using the molecular docking simulations demonstrates the stabilizing binding of their host-guest inclusion complexes, with the ΔG scores being all negative, suggesting that their formation can occur at room temperature. Corroborating the experimental outcomes, the computed 1,7-octadiyne complex has slightly more favored binding energy relative to the octane and 1,7-octadiene congeners. Moreover, DFT calculations based on the Energy Decomposition Analysis (EDA), reveal a key role of the electrostatic and dispersion energy in stabilizing the structures of the considered complexes. The stabilizing electrostatic contribution (ΔE_{elst}) is also predicted to be significantly higher for the complex 3 in comparison to the two other complexes 1 and 2 and increases with the ligand terminal carbon hybridization ($sp > sp^2 > sp^3$).

As expected, the increase of the dipole moment of the free guests is in line with the hybridization of the terminal carbon atom in these guests, $sp > sp^2 > sp^3$. The increase of the dipole moment of the host upon complexation is related to the enhancement of induced dipole-dipole interactions (van der Waals interactions) between guest and host molecules which are, in cooperative multiple noncovalent interactions, essential for realizing such strong complexations. Therefore, it is likely that the latter interactions play a significant role in stabilizing the inclusion process.

The corroborating results obtained using different DFT functionals for the binding energies, HOMO-LUMO pictures, and molecular electrostatic potential (MEP) plots indicate that the inclusion process is governed by the physical adsorption suggesting that the EtP5A can be used as a reversible (delivery) host for considered hydrocarbon molecules. Furthermore, the HOMO-LUMO energy gaps for the inclusion complexes are calculated to be lower for the host (EtP5A) than for the guests, which indicates that the

complex formation can be kinetically controllable. Notably, the NCI-RDG analysis shows that host-guest binding properties are mainly driven by weak stabilizing noncovalent interactions, *i.e.*, van der Waals forces (dispersion forces) and electrostatic C−H···π interactions that are responsible for the EtP5A slightly selective complexation towards the alkyne. This latter is favored by the higher electronegativity of the terminal carbon atom with the sp hybridization. The occurrence of H-bonding was shown to be unlikely in this case. The NBO intramolecular interaction analysis shows that, for all three complexes, there exist numerous stabilizing host→guest and guest→host intramolecular interactions. The former is represented by both π(C-C)→σ*(C–H) and LP(O)→σ*(C–H) type interactions, whereas the later are represented by different σ(C-H)→σ*(C–H), σ(C-H)→π*(C–C), π(C-C)→σ*(C–H) and σ(C-H)→ LP(C) type interactions in the complexes 1-3. These guest→host interactions energy in the complex 3 is found higher compared to the other complexes 1 and 2, further explaining its slightly higher binding energy.

Supporting Information

Supplementary data to this article can be found online.

Acknowledgments

We acknowledge the Algerian PRFU project (2022-2024: Grant No. B00L01EN250120220001) and the French GENCI IDRIS and GENCI-CINES for an allocation of computing time (Grant No. 2021-080649). Aleksey Kuznetsov appreciates the financial support of USM and computational facilities of the Department of Chemistry, ITA, Brazil.

Statements and Declarations

Funding: The authors have no relevant financial or non-financial interests to disclose.

Conflicts of interest/Competing interests:

The authors have no competing interests to declare that are relevant to the content of this article.

Availability of data and material: (data transparency):

All data generated or analyzed during this study are included in this published article [and its supplementary information files].

Code availability:

Commercial License

Amsterdam Molecular Simulation AMS2021: www.scm.com

Gaussian 09, Revision B.01: https://gaussian.com/

Open-source:

Avogadro Version 1.2.0n. http://avogadro.cc/

Molden Version 5.8.2: https://www.theochem.ru.nl/molden/

Multiwfn: http://sobereva.com/multiwfn/

AutoDock and AutoDockTools: http://autodock.scripps.edu ; http://mgltools.scripps.edu/downloads

Aleksey Kuznetsov appreciates computational facilities of the Department of Chemistry, ITA, Brazil.

Authors contributions:

Adel Krid: Conceptualization, Investigation, Material preparation, data collection. **Lotfi Belkhiri**: Formal analysis, Project administration, Supervision, Writing – original draft. **Hamza Allal**: Methodology, Software, Validation. **Aleksey Kuznetsov**: Conceptualization, Writing – original draft, Supervision, Investigation, Data collection, Software. Validation. **Abdou Boucekkine**: Writing – review & editing, Supervision.

References:

1. Zhang, Z., Luo, Y., Chen, J., Dong, S., Yu, Y., Ma, Z., Huang, F.: Formation of linear supramolecular polymers that is driven by C–H···π interactions in solution and in the solid state. Angew Chem Int Ed 50:1397–1401 (2011). https://doi.org/10.1002/anie.201006693
2. Ma, X., Zhao, Y.: Biomedical Applications of Supramolecular Systems Based on Host–Guest Interactions. Chem Rev 115:7794 (2015). https://doi.org/10.1021/cr500392w
3. Kataev, E.A.: Non-Covalent Interactions in the Synthesis of Macrocycles. In *Non-covalent Interactions in the Synthesis and Design of New Compounds*; John Wiley & Sons Ltd; pp 63–82 (2016). https://doi.org/10.1002/9781119113874.ch4
4. Zhou, J., Yu, G., Huang, F.: Supramolecular Chemotherapy Based on Host-Guest Molecular Recognition; A Novel Strategy in the Battle against Cancer with a Bright Future. Chem Soc Rev 46:7021–7053 (2017). https://doi.org/10.1039/C6CS00898D.
5. Wang, Z., Liu, Y.A., Yang, H., Hu, W.-B., Wen, K.: ortho-Functionalization of Pillar[5]arene: An Approach to Mono-ortho-Alkyl/Aryl-Substituted A1/A2-Dihydroxypillar[5]arene. Org Lett 24:1822–1826 (2022). https://doi.org/10.1021/acs.orglett.2c00272
6. Guo, L., Du, J., Wang, Y. Shi, K., Ma, E.: Advances in diversified application of pillar[n]arenes. J Incl Phenom Macrocycl Chem 97, 1–17 (2020). https://doi.org/10.1007/s10847-020-00986-z
7. Ogoshi, T., Kanai, S., Fujinami, S., Yamagishi, T., Nakamoto, Y.: Para-bridged symmetrical pillar[5]arenes: their Lewis acid catalyzed synthesis and host-guest property. J Am. Chem Soc

130:5022– 5023 (2008). https://doi.org/10.1021/ja711260m

8. Cragg, P.J., Sharma, K.: Pillar[5]arenes: Fascinating cyclophanes with a bright future. Chem Soc Rev 41:597–607 (2012). https://doi.org/10.1039/C1CS15164A
9. Nan, S., Ying-Wei, Y.: Applications of pillarenes, an emerging class of synthetic macrocycles, Sci China Chem 57:1185–1198 (2014). https://doi.org/10.1007/s11426-014-5190-z
10. Suvitha, A., Venkataramanan, N. S.: Trapping of organophosphorus chemical nerve agents by pillar[5] arene: A DFT, AIM, NCI and EDA analysis, J Incl Phenom Macrocycl Chem 87:207–218 (2017). https://doi.org/10.1007/s10847-017-0691-y
11. Li, H., Yang, Y., Xu, F., Liang, T., Wen, H., Tian, W.: Pillararene-Based Supramolecular Polymers, Chem Commun 55 :271–285 (2019). https://doi.org/10.1039/C8CC08085B
12. Sun, J., Hou, Y., Dai, Y., Wu, Q., Dong, Y., Zhao, J., Liu, Q,: Fluorescence quenched and boosted by a-PET effect and host-guest complexation respectively in BODIPY-functionalized pillar[5]arene. Dyes and Pigments 188:109163 (2021). https://doi.org/10.1016/j.dyepig.2021.109163
13. Nierengarten, I., Holler, M., Rémy, M., Hahn, U., Billot, A., Deschenaux, R., Nierengarten, J.-F.: Grafting Dendrons onto Pillar[5]Arene Scaffolds, Molecules 26:2358 (2021). https://doi.org/10.3390/molecules26082358
14. Fan, Y., Hu, K., Nan, J., Shen, Y.: Tetraphenylethene-Embedded Pillar[5]arene and [15]Paracyclophane: Distorted Cavities and Host–Guest Binding Properties, Molecules 26:5915 (2021). https://doi.org/10.3390/molecules26195915
15. Yang, H.-L., Li, Z.-H., Liu, P.-P., Sun, X.-W., Wang, Z.-H, Yao, H., Zhang, Y.-M., Wei, T.-B., Lin, Q.: Metal-Free White Light-Emitting Fluorescent Material Based on Simple Pillar[5]arene-tripodal Amide System and Theoretical Insights on Its Assembly and Fluorescent Properties. Langmuir 36:13469−13476 (2020). https://dx.doi.org/10.1021/acs.langmuir.0c02120
16. Plumb, J.A., Venugopal, B., Oun, R., Gomez-Roman, N., Kawazoe, Y., Venkataramanan, N.S., Wheate, N.J.: Cucurbit[7]uril encapsulated cisplatin overcomes cisplatin resistance via a pharmacokinetic effect, Metallomics 4:561–567 (2012). https://doi.org/10.1039/C2MT20054F
17. Wheate, N.J., Limantoro, C.: Cucurbit[n]urils as excipients in pharmaceutical dosage forms, Supramol Chem 28:849–856 (2016). https://doi.org/10.1080/10610278.2016.1178746
18. Wang, K., Yang, Y.W., Zhang, S.X.: Research progress on the synthesis of pillar[n]arenes and their host-guest chemistry. Chem J Chin Univ 33:1–13 (2012). https://doi.org/10.3969/j.issn.0251-0790.2012.01.001
19. Cao, D., Meier, H.: Pillar[n]arenes: a novel, highly promising class of macrocyclic host molecules. Asian J Org Chem 3:244–262 (2014). https://doi.org/10.1002/ajoc.201300224

20. Tao, H., Cao, D., Liu, L., Kou, Y., Wang, L., Meier, H.: Synthesis and host-guest properties of pillar[6]arenes. Sci China Chem 55:223–228 (2012). https://doi.org/10.1007/s11426-011-4427-3
21. Lou, X., Chen, H., Jia, X., Li, C.: Complexation of Linear Aliphatic Ester. Aldehyde and ketone guests by per-ethylated Pillar[5]Arene. Chin J Chem 33:335–338 (2015). https://doi.org/10.1002/cjoc.201400889
22. Venkataramanan, N.S., Suvitha, A., Vijayaraghavan, A., Thamotharan, S.: Investigation of inclusion complexation of acetaminophen with pillar [5]arene: UV–Vis, NMR and quantum chemical study. Journal of Molecular Liquids 241:782–791 (2017). http://dx.doi.org/10.1016/j.molliq.2017.06.095
23. Ogoshi, T., Sueto, R., Yoshikoshi, K., Sakata, Y., Akine, S., Yamagishi, T.: Host-Guest Complexation of Perethylated Pillar[5]Arene with Alkanes in the Crystal State. Angew Chem Int Ed 54:9849–9852 (2015). https://doi.org/10.1002/anie.201503489.
24. Ogosh, T.., Hamada, Y, Sueto, R.., Sakata, Y, Akine, S., Moeljadi, A.M.P., Hirao, H., Kakuta, T., Yamagishi, T., Mizuno, M.: Host-Guest Complexation Using Pillar[5]Arene Crystals: Crystal-Structure Dependent Uptake. Release, and Molecular Dynamics of an Alkane Guest Chem Eur J 25:2497–2502 (2019). https://doi.org/10.1002/chem.201805733.
25. Li, C., Chen, S., Li, J.., Han, K, Xu, M.., Hu, B, Yu, Y., Jia, X.: Novel Neutral Guest Recognition and Interpenetrated Complex Formation from Pillar[5]Arenes. Chem Commun 47:11294–11296 (2011). https://doi.org/10.1039/C1CC14829J
26. Venkataramanan, N.S., Suvitha, A. & Kawazoe, Y. Unraveling the binding nature of hexane with quinone functionalized pillar[5]quinone: a computational study. J Incl Phenom Macrocycl Chem 95, 307–319 (2019). https://doi.org/10.1007/s10847-019-00945-3
27. Li, Z.-H., Yang, H.-L., Wei, T.-B., Lin, Q.: Investigation of the assembly mechanism of N1, N4-di (pyridin-4-yl) terephthalamide with pillar[5]arene: Experiment and quantum chemical study, Chem Phys Lett 772:138533 (2021). https://doi.org/10.1016/j.cplett.2021.138533
28. Li, F., Zhang, G., Xia, S., Yu, L.: Host-guest interactions accompanying the cationic nitrogen heterocyclic guests encapsulation within pillar[5]arene: A theoretical research. J Mol Struct 1198:126862 (2019). https://doi.org/10.1016/j.molstruc.2019.07.109
29. Ogoshi, T.: Synthesis of novel pillar-shaped cavitands “pillar[5]arenes” and their application for supramolecular materials. J Incl Phenom Macrocycl Chem 72:247–262 (2012). https://doi.org/10.1007/s10847-011-0027-2
30. Bhattacharyya, P.K.: Reactivity, aromaticity and absorption spectra of pillar[5]arene conformers: A DFT study. Comput Theor Chem 1066:20–27 (2015). http://dx.doi.org/10.1016/j.comptc.2015.05.007

31. Tan, L.L., Zhang, Y., Li, B., Wang, K., Zhang, X.A., Tao, Y., Yang, Y.W.: Selective recognition of “solvent” molecules in solution and the solid state by 1,4-dimethoxypillar[5]arene driven by attractive forces. New J Chem 38:845–851 (2014). https://doi.org/10.1039/C3NJ01498C
32. Shurpik, D.N., Stoikov, I. I.: Covalent Assembly of Tris-pillar[5]arene. Russ J Gen Chem 86:752–755 (2016). https://doi.org/10.1134/S1070363216030439
33. Xie, J., Zuo, T., Huang, Z., Huan, L., Gu, Q., Gao, C., Shao, J.: Theoretical study of a novel imino bridged pillar[5]arene derivative. Chem Phys Lett 662:25–30 (2016). http://dx.doi.org/10.1016/j.cplett.2016.09.010
34. Sharma, H., Deka, B.C., Saha, B., Bhattacharyya, P..K.: Understanding the structure, reactivity and absorption spectra of borazine doped pillar[5]arene: A DFT study. Comput Theor Chem 1139:82–89 (2018). https://doi.org/10.1016/j.comptc.2018.07.011
35. Athare, S.V., Gejji, SP.: Hydrogen Bonding versus H–H Interactions in Pillar[n]arenes, ChemistrySelect 4:9354 –9359 (2019). https://doi.org/10.1002/slct.201901984
36. Ogoshi, T.., Yamagishi T: Pillar[5] – and pillar[6]arene-based supramolecular assemblies built by using their cavity-size dependent host-guest interactions, Chem Commun 50:4776–4787 (2014). https://doi.org/10.1039/C4CC00738G
37. Kou, Y., Cao, D., Tao, H., Wang, L.., Liang, J, Chen, J., Meier, H.: Synthesis and inclusion properties of pillar[n]arenes. J Incl Phenom Macrocycl Chem 77:279–289 (2013). https://doi.org/10.1007/s10847-012-0242-5
38. Ogoshi, T., Yamagishi, T.: Pillar[5]- and pillar[6]arene-based supramolecular assemblies built by using their cavity-size-dependent host-guest interactions. Chem Commun 50:4776–4787 (2014). https://doi.org/10.1039/C4CC00738G
39. Wang, Y., Ping, G., Li, C.: Efficient complexation between pillar[5]arenes and neutral guests: from host-guest chemistry to functional materials, Chem Commun 32:9858–9872 (2016). https://doi.org/10.1039/C6CC03999E
40. Li, C., Zhao, L., Li, J., Ding, X., Chen, S., Zhang, Q., Yu, Y., Jia, X.: Self-Assembly of [2]Pseudorotaxanes Based on Pillar[5]Arene and Bis(Imidazolium) Cations. Chem Commun 46:9016–9018 (2010). https://doi.org/10.1039/C0CC03575K
41. Shu, X., Fan, J., Li, J., Wang, X., Chen, W., Jia, X., Li, C.: Complexation of Neutral 1.4-Dihalobutanes with Simple Pillar[5]Arenes That Is Dominated by Dispersion Forces. Org Biomol Chem 10:3393–3397 (2012). https://doi.org/10.1039/C2OB25251A
42. Athare, S.V., Gejji, S.P.: Probing Binding of Ethylated Pillar[5]arene with Pentene and Chlorobutane Positional Isomers. J Phys Chem A 123:8391–8396 (2019).

https://doi.org/10.1021/acs.jpca.9b05563

43. Panneerselvam, M., Kumar, M.D., Jaccob, M., Solomon, R.V.: Computational Unravelling of the Role of Alkyl Groups on the Host-Guest Complexation of pillar[5]arenes with Neutral Dihalobutanes. ChemistrySelect 3:1321−1334 (2018). https://doi.org/10.1002/slct.201702541
44. Hu, X.-S., Deng, H.-M., Li, J., Jia, X.-S., Li, C.-J.: Selective Binding of Unsaturated Aliphatic Hydrocarbons by a Pillar[5]Arene. Chin Chem Lett 24:707–709 (2013). https://doi.org/10.1016/j.cclet.2013.05.008
45. Jie, K., Zhou, Y., Li, E., Zhao, R., Liu, M., Huang, F.: Linear Positional Isomer Sorting in Nonporous Adaptive Crystals of a Pillar[5]arene. J Am Chem Soc 140:3190−3193 (2018). https://doi.org/10.1021/jacs.7b13156
46. Trott, O., Olson, A.J.: AutoDock Vina: Improving the Speed and Accuracy of Docking with a New Scoring Function. Efficient Optimization. and Multithreading. J Comput Chem 31:455–461 (2010). https://doi.org/10.1002/jcc.21334
47. Morris, G.M., Huey, R., Lindstrom, W., Sanner, M.F., Belew, R.K., Goodsell, D.S., Olson, A. J.: AutoDock4 and AutoDockTools4: Automated Docking with Selective Receptor Flexibility. J Comput Chem 30:785–2791 (2009). https://doi.org/10.1002/jcc.21256
48. te Velde, G., Bickelhaupt, F. M., Baerends, E. J., Guerra, C. F., van Gisbergen, S. J. A., Snijders, J. G., Ziegler, T.: Chemistry with ADF. J Comput Chem 22:931–967(2001). https://doi.org/10.1002/jcc.1056
49. ADF 2021.107, SCM, Theoretical Chemistry, Vrije Universiteit, Amsterdam, The Netherlands, http://www.scm.com. E.J. Baerends, T. Ziegler, A.J. Atkins, J. Autschbach, O. Baseggio, D. Bashford, A. Bérces, F.M. Bickelhaupt, C. Bo, P.M. Boerrigter, L. Cavallo, C. Daul, D.P. Chong, D.V. Chulhai, L. Deng, R.M. Dickson, J.M. Dieterich, D.E. Ellis, M. van Faassen, L. Fan, T.H. Fischer, A. Förster, C. Fonseca Guerra, M. Franchini, A. Ghysels, A. Giammona, S.J.A. van Gisbergen, A. Goez, A.W. Götz, J.A. Groeneveld, O.V. Gritsenko, M. Grüning, S. Gusarov, F.E. Harris, P. van den Hoek, Z. Hu, C.R. Jacob, H. Jacobsen, L. Jensen, L. Joubert, J.W. Kaminski, G. van Kessel, C. König, F. Kootstra, A. Kovalenko, M.V. Krykunov, E. van Lenthe, D.A. McCormack, A. Michalak, M. Mitoraj, S.M. Morton, J. Neugebauer, V.P. Nicu, L. Noodleman, V.P. Osinga, S. Patchkovskii, M. Pavanello, C.A. Peeples, P.H.T. Philipsen, D. Post, C.C. Pye, H. Ramanantoanina, P. Ramos, W. Ravenek, J.I. Rodríguez, P. Ros, R. Rüger, P.R.T. Schipper, D. Schlüns, H. van Schoot, G. Schreckenbach, J.S. Seldenthuis, M. Seth, J.G. Snijders, M. Solà, M. Stener, M. Swart, D. Swerhone, V. Tognetti, G. te Velde, P. Vernooijs, L. Versluis, L. Visscher, O. Visser, F. Wang, T.A. Wesolowski, E.M. van Wezenbeek, G. Wiesenekker, S.K. Wolff, T.K. Woo, A.L. Yakovlev.

50. Frisch, M.J., Trucks, G.W., Schlegel, H.B., Scuseria, G.E., Robb, M.A., Cheeseman, J.R., Scalmani, G., Barone, V., Petersson, G.A., Nakatsuji, H., Li, X., Caricato, M., Marenich, A.V., Bloino, J., Janesko, B.G., Gomperts, R., Mennucci, B., Hratchian, H.P., Ortiz, J.V., Izmaylov, A.F., Sonnenberg, J.L., Williams-Young, D., Ding, F., Lipparini, F., Egidi, F., Goings, J., Peng, B., Petrone, A., Henderson, T., Ranasinghe, D., Zakrzewski, V.G., Gao, J., Rega, N., Zheng, G., Liang, W., Hada, M., Ehara, M., Toyota, K., Fukuda, R., Hasegawa, J., Ishida, M., Nakajima, T., Honda, Y., Kitao, O., Nakai, H., Vreven, T., Throssell, K., Montgomery Jr., J.A., Peralta, J.E., Ogliaro, F., Bearpark, M.J., Heyd, J.J., Brothers, E.N., Kudin, K.N., Staroverov, V.N., Keith, T.A., Kobayashi, R., Normand, J., Raghavachari, K., Rendell, A.P., Burant, J.C., Iyengar, S.S., Tomasi, J., Cossi, M., Millam, J.M., Klene, M., Adamo, C., Cammi, R., Ochterski, J.W., Martin, R.L., Morokuma, K., Farkas, O., Foresman, J.B., Fox, D.J.: Gaussian 09, Revision B.01. Gaussian Inc, Wallingford (2010)
51. Mirzaeva, I.V., Kovalenko, E. A., Fedin, V. P.: Theoretical Study of Host–Guest Interactions in Complexes of Cucurbit[7]Uril with Protonated Amino Acids. Supramolecular Chemistry. 28:857–863 (2016). https://doi.org/10.1080/10610278.2016.1194420
52. Becke, A. D.: Density-Functional Exchange-Energy Approximation with Correct Asymptotic Behavior. Phys. Rev. A. 38:3098–3100 (1988). https://doi.org/10.1103/PhysRevA.38.3098
53. Grimme, S., Ehrlich, S., Goerigk, L.: Effect of the Damping Function in Dispersion Corrected Density Functional Theory. J Comput Chem 32:1456–1465 (2011). https://doi.org/10.1002/jcc.21759.
54. Goerigk, L., Hansen, A., Bauer, C., Ehrlich, S., Najibi, A., Grimme, S.: A Look at the Density Functional Theory Zoo with the Advanced GMTKN55 Database for General Main Group Thermochemistry. Kinetics. and Noncovalent Interactions. Phys Chem Chem Phys 19:32184–32215 (2017). https://doi.org/10.1039/C7CP04913G
55. Pye, C. C., Ziegler, T.: An Implementation of the Conductor-like Screening Model of Solvation within the Amsterdam Density Functional Package. Theor Chem Acc 101:396–408 (1999). https://doi.org/10.1007/s002140050457
56. Lu, T., Chen, F.: Multiwfn, A Multifunctional Wavefunction Analyzer, J Comp Chem 33:580–592 (2012). https://doi.org/10.1002/jcc.22885
57. Humphrey, W., Dalke, A., Schulten, K.: VMD - Visual Molecular Dynamics, J Mol Graphics 14:33-38 (1996). http://www.ks.uiuc.edu/Research/vmd/
58. Mitoraj, M. P., Michalak, A., Ziegler, T.: A Combined Charge and Energy Decomposition Scheme for Bond Analysis. J Chem Theo Comput 5: 962–975 (2009). https://doi.org/10.1021/ct800503d
59. Morokuma, K.: Molecular Orbital Studies of Hydrogen Bonds. III. C=O···H–O Hydrogen Bond in $H_2CO\cdots H_2O$ and $H_2CO\cdots 2H_2O$. J Chem Phys 55:1236 (1971). https://doi.org/10.1063/1.1676210

60. Pan, S., Saha, R., Mandal, S., Mondal, S., Gupta, A., Gernández, M. H., Merino, G., Chattaraj, P. K.: Selectivity in gas adsorption by molecular cucurbit[6]uril, J Phys Chem C 120:13911–13921 (2016). https://doi.org/10.1021/acs.jpcc.6b02545

61. Bhadane, S.A., Lande, D.N., Gejji, S.P.: Understanding binding of cyano-adamantyl derivatives to pillar[6]arene macrocycle from density functional theory, J Phys Chem A 120:8738–8749 (2016). https://doi.org/10.1021/acs.jpca.6b08512

62. Chain, J.-D., Head-Gordon, M.: Long-range corrected hybrid density functionals with damped atom-atom dispersion corrections, Phys Chem Chem Phys 10:6615-20 (2008). https://doi.org/10.1039/B810189B

63. Grimme, S.: Semiempirical GGA-type density functional constructed with a long-range dispersion correction, J Comp Chem 27:1787-99 (2006). https://doi.org/10.1002/jcc.20495

64. McLean A. D., Chandler G. S.: Contracted Gaussian-basis sets for molecular calculations. 1. 2nd row atoms, Z=11-18, J Chem Phys 72:5639-48 (1980). https://doi.org/10.1063/1.438980

65. Raghavachari, K., Binkley, J. S., Seeger, R., Pople, J.A.: Self-Consistent Molecular Orbital Methods. 20. Basis set for correlated wave-functions, J Chem Phys 72:650-54 (1980). https://doi.org/10.1063/1.438955

66. Tomasi, J., Mennucci, B., Cammi, R.: Quantum mechanical continuum solvation models. Chem Rev 105 2999-3093 (2005). https://doi.org/10.1021/cr9904009

67. Reed, A.E., Curtiss, L.A., Weinhold, F.: Intermolecular interactions from a natural bond orbital, donor-acceptor viewpoint. ChemRev. 88:899-926 (1988). https://doi.org/10.1021/cr00088a005

68. Schaftenaar, G., Noordik, J.H.: Molden, a pre- and post-processing program for molecular and electronic structures. J. Comput Aided Mol Design. 14:123-134 (2000). https://doi.org/10.1023/A:1008193805436

69. Avogadro: an open-source molecular builder and visualization tool. Version 1.2.0n. http://avogadro.cc/

70. Hanwell, M.D., Curtis, D.E., Lonie, D.C., Vandermeersch, T., Zurek, E., Hutchison, G.R.: Avogadro: an advanced semantic chemical editor, visualization, and analysis platform, J Cheminformatics 41:1–17 (2012). https://doi.org/10.1186/1758-2946-4-17.

71. Khedkar, J.K., Jagtap, K.K., Pinjari, R.V., Ray, A.K., Gejji, S.P.: Binding of rhodamine B and kiton red S to cucurbit[7]uril: density functional investigations, J Mol Model 18:743–3750 (2012). https://doi.org/10.1007/s00894-012-1375-6

72. Venkataramanan, N.S., Suvitha, A.: Theoretical investigation of the binding of nucleobases to cucurbiturils by dispersion corrected DFT approaches, J Phys Chem B 121:4733–4744 (2017).

https://doi.org/10.1021/acs.jpca.6b10310

73. Shewale, M.N., Lande, D.N., Gejji, S.P.: Encapsulation of benzimidazole derivatives within cucurbit[7]uril: density functional investigations, J Mol Liq 216:309–317 (2016). https://doi.org/10.10c16/j.molliq.2015.12.076

74. Murry, J.S., Seminario, J.M., Politzer, P.: A computational study of the structures and electrostatic potentials of some azines and nitroazines. J Mol Struct: THEOCHEM 187:95−108 (1989). https://doi.org/10.1016/0166-1280(89)85152-8

75. Silva, D.S., Oliveria, B.G.: New insights about the hydrogen bonds formed between acetylene and hydrogen fluoride: π···H, C···H and F···H, Spectrosc. Chem Acta A Mol Biomo 173:160–169 (2017). https://doi.org/10.1016/j.saa.2016.08.054

76. Lakshmipriya, A., Suryaprakash, N.: Two- and three-centered hydrogen bonds involving organic fuorine stabilize conformations of hydrazide halo derivatives: NMR, IR, QTAIM, NCI, and theoretical evidence, J Phys Chem A 120:7810–7816 (2016). https://doi.org/10.1021/acs.jpca.6b06362